Journal of Hydrology 590 (2020) 125499

Contents lists available at ScienceDirect

Journal of Hydrology

journal homepage: www.elsevier.com/locate/jhydrol

Research papers

Validation of remotely sensed estimates of snow water equivalent using multiple reference datasets from the middle and high latitudes of China

J.W. Yang[a], L.M. Jiang[a,*], J. Lemmetyinen[b], K. Luojus[b], M. Takala[b], S.L. Wu[d], J.M. Pan[c]

[a] State Key Laboratory of Remote Sensing Science, Jointly Sponsored by Beijing Normal University and Aerospace Information Research Institute of Chinese Academy of Sciences, Faculty of Geographical Science, Beijing Normal University, Beijing 100875, China
[b] Finnish Meteorological Institute, Helsinki Fi00101, Finland
[c] State Key Laboratory of Remote Sensing Science, Aerospace Information Research Institute, Chinese Academy of Sciences, Beijing 100101, China
[d] National Satellite Meteorological Center, China Meteorological Administration, Beijing 100081, China

ARTICLE INFO

This manuscript was handled by Marco Borga, Editor-in-Chief, with the assistance of Massimiliano Zappa, Associate Editor

Keywords:
Snow water equivalent (SWE)
GlobSnow-2
Multiple reference datasets
China

ABSTRACT

A key variable describing the mass of seasonal snow cover is snow water equivalent (SWE), which plays an important role in hydrological applications, weather forecasting and land surface process simulations. In this paper, the accuracy of an SWE product, GlobSnow-2, which combines microwave satellite data and in situ measurements, is assessed using three reference evaluation datasets north of 35°N in China. The GlobSnow-2 estimates are also compared with stand-alone satellite products (AMSR2, Chang and FY-3D SWE). The overall unbiased root mean square error (RMSE) and bias of the GlobSnow-2 SWE product validated with three reference datasets are 17.4 mm and 11.2 mm, respectively, which outperforms the AMSR2 SWE (39.3 mm and 37.3 mm, respectively) and Chang SWE (57.5 mm and 46.2 mm, respectively) products. The FY-3D SWE product performs better than the GlobSnow-2 estimate for shallow snow (SWE < 50 mm) and tends to underestimate snow cover, particularly when SWE exceeds 80 mm. A retrieval sensitivity analysis against land cover types shows that the highest SWE uncertainties for GlobSnow-2 are exhibited in grassland (unbiased RMSE, 27.8 mm), and the most serious overestimation occurs in forested areas (bias, 23.6 mm). The GlobSnow-2 performances at various elevations show an increasing bias trend, ranging from 5 to 61 mm with increasing elevation. The GlobSnow-2 estimate analyses under different snow regimes show that the GlobSnow-2 SWE product performs best in taiga snow, with high uncertainties (unbiased RMSE, 28.3 mm) in prairie snow and serious overestimations (bias, 23.2 mm) for alpine snow. The results of this study demonstrate that the GlobSnow-2 assimilation approach tends to overestimate SWE in China. One of the major reasons that overestimations occur is that the GlobSnow-2 SWE retrieval scheme utilizes a fixed density of 240 kg/m^3, which is larger than the average value derived from ground measurements for China (180 kg/m^3), which undoubtedly contributes to the observed SWE overestimation. Another reason is that forest effects on satellite signals remain challenging for SWE estimations in the GlobSnow-2 assimilation system. The retrieval errors in prairie and alpine are also higher than others due to the snowpack stratigraphy and complex topography. The GlobSnow-2 SWE product performance is evaluated over China in this study, and the major factors that affect the assimilation scheme accuracy are determined. These results will provide a reference to improve the GlobSnow-2 SWE product in future work.

1. Introduction

Seasonal snow covers nearly 50% of terrestrial areas in the Northern Hemisphere during winter (Brown and Robinson, 2011; Bormann et al., 2018). Snow cover is the largest single component of the cryosphere in terms of spatial extent and it affects the global surface energy balance due to its high albedo and the energy allocation involved in the snow melting (Hansen and Nazarenko, 2004; Li et al., 2018). The amount of water stored in a snowpack, which is obtained as snow water equivalent (SWE), is of great importance for hydrological applications, numerical weather predictions, climate change research and land surface process simulations (Derksen et al., 2010; Qin et al., 2020). Snowmelt runoff not only supports the water demands of approximately a sixth of the Earth's population (~1.4 billion people) but also directly affects agricultural and ecological systems in downstream areas (Barnett et al., 2005). At the same time, accurate forecasting of this water supply is

* Corresponding author.
E-mail address: jiang@bnu.edu.cn (L.M. Jiang).

https://doi.org/10.1016/j.jhydrol.2020.125499
Received 16 February 2020; Received in revised form 21 August 2020; Accepted 31 August 2020
Available online 11 September 2020

essential for the optimal management of snowmelt and prevention of natural hazards such as flooding and avalanches (Bartelt and Lehning, 2002; Vormoor et al., 2015; Larue et al., 2017; Pulliainen et al., 2020).

There exist three major snow cover regions in China, including Northeast China, northern Xinjiang and the Qinghai-Tibetan Plateau, where the mean snow cover extent during the winter covers 27% of the country's total area (Huang et al., 2016). The Xinjiang province locates on the northwest of China, dominated by the grassland and bare ground (Ran et al., 2012). Snow covers are mainly distributed in northern Xinjiang, especially around the Altai and Tian Shan mountains (Dai et al., 2012; Zhong et al., 2018). Previous studies have shown that the average annual snow depth in northern Xinjiang is highest among these three snow-covered areas in China (Huang et al., 2019; Yang et al., 2020). In Northeast China, the forest cover accounts for 40% of the total area (Che et al., 2016). Meanwhile, the topography in Northeast China is complex due to many existing mountains, e.g., Great Khingan, Lesser Khingan, and Changbai. They are the forest and mountain covered regions in Northeast China that are covered with relatively deep snowpacks (Zhong et al., 2018; Huang et al., 2019). The Qinghai-Tibetan Plateau is the region with an average elevation of more than 4000 m. The average annual snow depth in the Qinghai-Tibetan Plateau is smallest among three major snow cover regions, with a mean value of approximately 5 cm (Dai et al., 2018; Wang et al., 2019). However, the annual maximum snow depth typically occurs in the southwest of Qinghai-Tibetan Plateau, known as the Himalaya range (Dai et al., 2017; Yang et al., 2020).

Satellite passive microwave (PMW) remote sensing has been proposed as an efficient way to retrieve SWE at both global and regional scales (Armstrong and Brodzik, 2002; Foster et al., 2011; Hancock et al., 2013; Tedesco and Narvekar, 2010). The physical basis behind PMW SWE retrievals is that the volume scattering of microwave radiation in snow varies with wavelength; thus, the contrast between microwave brightness temperature at K- (~19 GHz) and Ka-band (~37 GHz) can be related to the amount of snow in the radiation propagation path (Chang et al., 1987; Mätzler, 1994; Tedesco et al., 2004). PMW remote sensing is less affected by atmospheric conditions than optical sensors and provides Earth observation capability during day and night at good temporal (daily) and moderate spatial (~25 km) resolutions (Chang et al., 1987). Another advantage of microwaves over optical wavelengths is the possibility of extracting information for the whole snowpack and not just the surface (Lemmetyinen et al., 2016; Zheng et al., 2016).

Diverse methods have been proposed to retrieve SWE using PMW observations, including static and dynamic semiempirical algorithms (Chang et al., 1987; Foster et al., 1997, 2005; Kelly et al., 2003; Kelly, 2009; Derksen et al., 2005; Jiang et al., 2014), physically based statistical methods (Jiang et al., 2007, 2011; Dai et al., 2012; Picard et al., 2013; Che et al., 2016; Pan et al., 2017), machine learning approaches (Santi et al., 2012, 2014; Durand and Liu, 2012; Forman and Reichle, 2015; Bair et al., 2018; Yang et al., 2020) and assimilation techniques (Sun et al., 2004; Pulliainen, 2006; Durand et al., 2009; Tedesco and Narvekar, 2010; Li et al., 2012, 2017; Xue et al., 2018; Kim et al., 2019; Pulliainen et al., 2020). Most of the widely used inversion algorithms are based on empirical or semiempirical relationships between snow depth and multifrequency spaceborne satellite brightness temperature gradients. In China, two static snow depth algorithms were originally developed based on Chinese weather station observations and PMW brightness temperatures (Che et al., 2008; Jiang et al., 2014). The algorithm proposed by Che et al. (2008) is the revised Chang algorithm. It has been used to generate a long-term snow dataset for the algorithm of the Environmental and Ecological Science Data Centre of Western China (hereafter, WESTDC product). The mixed-pixel approach proposed by Jiang et al. in 2014 was designed for China's Fenyun-3B satellite (FY-3B), considering the influence of land cover types on SWE retrieval according to the Derksen et al. study in 2005. The accuracy of these empirical or semiempirical approaches is affected by uncertainties arising from several simplifications. One such simplification is that snow grain size (radius) and snow density are typically assumed to be uniform throughout snowpack (Armstrong and Brodzik, 2002). Other sources of uncertainty are related to the effects of the forest canopy and atmosphere (Foster et al., 2005; Derksen and Brown, 2012; Roy et al., 2014; Shi et al., 2017). The current JAXA standard SWE algorithm designed for the Advanced Microwave Scanning Radiometer 2 (AMSR2) onboard the GCOM-W1 satellite accounts for the influence of forest cover and snow grain growth and takes advantage of the expanded range of channels (10.65, 18.7 and 36.5 GHz) available on the AMSR2 instruments (Kelly, 2009). Yang et al. (2019) assessed the AMSR2 algorithm in addition to four other methods over China using weather station observations. The validation results indicated that the Chang algorithm (Chang et al., 1987) and AMSR2 algorithm tend to overestimate snow depth over China, with biases as high as 14 cm and 8.7 cm, respectively. However, underestimation of SWE was reported for the FY-3B (Jiang et al., 2014) and WESTDC (Che et al., 2008) algorithms when snow cover was thicker than 20 cm. The Foster algorithm accounts for the influence of forest cover on brightness temperature (Foster et al., 1997). However, it tends to overestimate snow depth in China, especially in densely forested areas (Gu et al., 2018; Yang et al., 2019).

A technique that assimilates in situ snow depth observations with microwave emissions by means of a forward emission model for snow was proposed by Pulliainen in 2006. This assimilation approach was applied in the European Space Agency's (ESA) GlobSnow project to estimate daily SWE time series from 1979 to present over the Northern Hemisphere (Takala et al., 2011).

The GlobSnow-2 SWE algorithm has three features compared to empirical and semiempirical methods. First, the approach considers atmospheric and forest effects on spaceborne observed brightness temperature by means of the forest transmissivity model by Pulliainen et al (1993) and the statistical atmospheric model in Kruopis et al (1999). It is commonly acknowledged that forest canopies attenuate PMW radiation emitted from the underlying snowpack and simultaneously contribute to their own signal (Foster et al., 2005; Langlois et al., 2011). The forest canopy microwave transmissivity is strongly correlated with structural parameters (such as stem volume and canopy density), canopy intercepted snow, snow cover class and frequency (Gelfan et al., 2004; Lemmetyinen et al., 2009; Roy et al., 2014; Xue and Forman, 2017; Cai et al., 2017). A newly published study also highlights the sensitivity of canopy transmissivity to tree skin temperature (Li et al., 2019). Previous studies conducted from observation and modeling perspectives have indicated that forest transmissivity values decreased spectrally from 0.80 to 0.40 for frequencies ranging from 6.9 to 37 GHz (Langlois et al., 2011; Roy et al., 2014; Vander Jagt et al., 2015; Che et al., 2016; Li et al., 2017). Forests cover 40% of Northeast China, which is one of the three primary snow-covered regions in China. Che et al. (2016) compared three satellite SWE products, the AMSR2 standard product, the GlobSnow-2 SWE product and the WESTDC product over Northeast China. The results showed that the GlobSnow-2 estimate was superior to the WESTDC product and NASA product estimates in forest regions, although the relative error was as high as 60%.

The second feature is that the GlobSnow-2 algorithm assimilates spaceborne PMW remote sensing data with synoptic weather station observations of snow depth. It has been demonstrated that the assimilation of PMW satellite data and in situ observations (snow depth, SWE and snow cover fraction) into snow models is a promising approach used to improve SWE estimation (Pulliainen, 2006; Durand et al., 2009; Xu et al., 2014; Kwon et al., 2017; Larue et al., 2018). Li et al. (2017) assimilated the AMSR-E 36.5 GHz observations into the microwave emission model of layered snowpack (MEMLS) model simulations of SWE using the ensemble batch smoother (EBS) data assimilation method. In this study, a Land Surface Model (LSM) provided prior estimates of the state variables for the MEMLS model. After assimilation,

the overall root-mean-square error (RMSE) of the SWE estimates was reduced by 35.4%, and the bias was reduced by 84.2%. Magnusson et al. (2017) used the particle filter algorithm to assimilate snow depth measurements into a multilayer energy balance snow model to improves the estimates. The results showed that the assimilation method make the RMSE of SWE estimates reduce by 64% compared to the model without assimilation. Larue et al. (2018) suggested that the overall SWE RMSE was reduced by 82% compared to the original SWE simulations through the assimilation of AMSR2 observations into a microwave snow forward model by using the particle filter assimilation scheme. Stigter et al. (2017) found that the assimilation of snow cover and snow depth into the modified seNorge snow model using the Kalman filter technique also improved the estimate of SWE in a Himalayan catchment. Therefore, data assimilation can contribute to ensure that model simulations remain close to ground truth values, which corrects the effects of potential errors in modeling and inputs on SWE estimates (Kumar et al., 2015; Magnusson et al., 2017).

A third feature of the GlobSnow-2 algorithm is the optimization of effective snow grain size, which fits forward model simulations to the satellite brightness temperature observations. One of the major challenges for SWE estimation using PMW remote sensing data is the effect of snow microstructure (e.g., grain size and shape and moisture content) on microwave radiation originating from soil (Roy et al., 2004; Langlois et al., 2012; Picard et al., 2013; Kontu et al., 2017; Pan et al., 2016). Previous studies have proven that the snow microstructure and snow grain size are the most sensitive parameters affecting the extinction coefficient of snowpack (Hallikainen et al., 1987; Tedesco and Kim, 2006; Lemmetyinen et al., 2015; Kontu et al., 2017; Picard et al., 2018). Even small changes in the size of scattering particles notably modify the measured brightness temperature. The optimized grain size in GlobSnow-2 is actually an effective value that includes the effects of modeling errors and uncertainties in input data (snow density, snow grain size and forest stem volume).

At present, there are two widely used global (AMSR2 and GlobSnow-2) and two regional (WESTDC and FY-3) SWE products available in China (see Section 2.2). These SWE datasets can also be classified into stand-alone satellite (AMSR2, WESTDC, FY-3) and assimilated (GlobSnow-2) products. Previous studies have demonstrated that these stand-alone satellite global SWE products tend to overestimate SWE in China (Dai et al., 2012; Yang et al., 2015, 2019; Gu et al., 2016; Zhang et al., 2017; Wang et al., 2019). The regional SWE products (e.g., WESTDC and FY-3B) designed for China presented similar performance, and outperformed global SWE products (Li et al., 2014; Gu et al., 2018; Yang et al., 2019). The assimilated GlobSnow-2 SWE historical dataset is freely available (see www.globsnow.info), and its gridded SWE data are potentially of great interest in studies of climate change, hydrological processes, permafrost changes, vegetation growth and river runoff (Che et al., 2016; Larue et al., 2017; Pulliainen et al., 2017). Previous assessments suggested that GlobSnow-2 estimates can approach the reanalysis-based products regarding accuracy over the Northern Hemisphere regions, outperforming the other stand-alone satellite SWE products (Mudryk et al., 2015; Jeong et al., 2017; Mortimer et al., 2020). However, while the GlobSnow-2 SWE algorithm exhibits some advantages in its methodology compared with other empirical and semiempirical methods, its performance over China has never been studied in detail.

The main purpose of this paper is to thoroughly assess the GlobSnow-2 SWE product over China using multireference datasets from weather stations, snow course surveys and field sampling, determining the main factors affecting the performance of the GlobSnow-2 SWE product in China. The results of this paper will serve to improve SWE estimates of the GlobSnow-2 retrieval scheme in the near future.

2. Material and methods

Three validation datasets from stations, snow survey courses and field sampling were used to verify the GlobSnow-2 SWE product. It was also compared with other widely used SWE products, including the AMSR2 SWE product, FY-3D SWE product, and Chang SWE product. Meanwhile, to consider the influence of snow cover characteristics on SWE estimation, the assessment of GlobSnow-2 SWE product was performed in various climatological snow classes according to the Sturm et al. (1995) seasonal snow classification. In addition, a GlobSnow-2 retrieval sensitivity analysis was conducted against land cover types and elevation.

2.1. Ground observations

Three validation datasets available for assessing the GlobSnow-2 SWE product are briefly introduced in the following section.

A) Weather station measurements (*Dataset 1*): The weather station data were acquired from the National Meteorological Information Centre, China Meteorology Administration (CMA, http://data.cma.cn/en). The recorded variables include the site name, observation time, geolocation (latitude and longitude), elevation (m), near surface soil temperature (measured at a 5 cm depth, ˚C), snow depth (cm), and snow pressure (g/cm^2), which are applied to yield SWE. *Dataset 1* covers 297 stations (only north of 35˚N, which is the same as the extent of the GlobSnow-2 product) throughout China from 2014 to 2017 (Fig. 1, left). The dataset covers northern Xinjiang and Northeast and central China, which are the primary stable snow-covered regions in China (Fig. 1, right). Most observations are distributed in northern

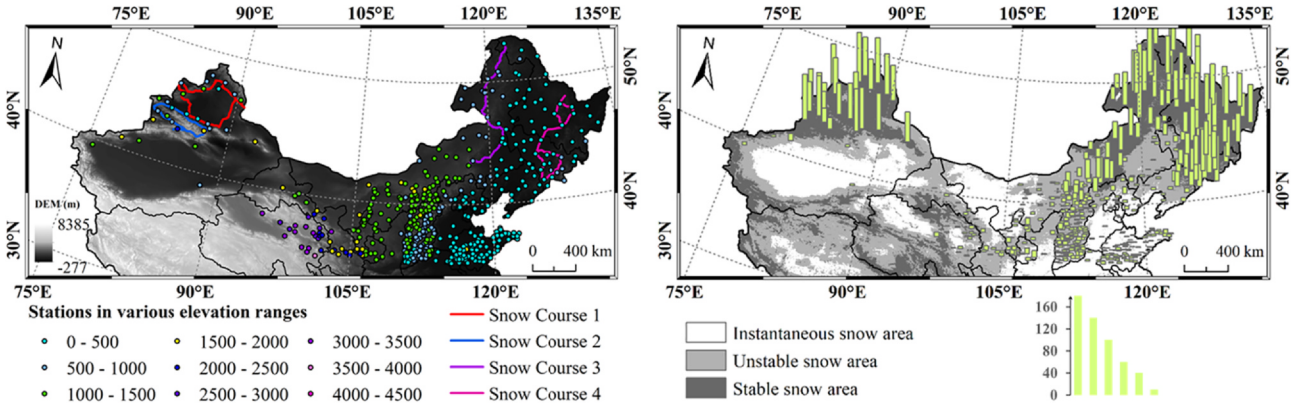

Fig. 1. Spatial distribution of weather stations (left) and snow cover types (right) in China. The four colored lines are the snow course routes spanning from December 2017 to March 2018. The base map on the left shows digital elevation model (DEM) data with a 90 m resolution, collected from Data Center for Resources and Environmental Sciences, Chinese Academy of Sciences (http://www.resdc.cn/). The histogram on the right indicates the number of observations for each weather station during the 2014–2017 period.

Table 1
Summary of snow course data (location, air temperature, snow depth, snow density, the number of samples, and snow class).

Snow course	Location (lat, lon)	Air temperature (°C)			Snow depth (cm)			Snow density (kg/m^3)			Snow class	Samples
		Max	Min	Mean	Max	Min	Mean	Max	Min	Mean		
1	43.90°N–48.06°N 82.97°E–89.88°E	–1.7	–34.0	–18.8	50.0	3.0	13.2	300	100	180	tundra taiga prairie	70
2	42.97°N–44.50°N 80.83°E–88.97°E	–0.6	–29.5	–12.9	63.0	3.0	19.8	410	120	210	prairie alpine	73
3	45.10°N–53.46°N 118.30°E–126.96°E	–1.5	–33.8	–15.8	51.5	3.2	16.4	310	60	160	prairie taiga tundra	100
4	41.88°N–48.17°N 125.73°E–130.31°E	–3.1	–30.6	–12.4	45.2	4.1	16.6	240	150	180	taiga alpine	54

Xinjiang and Northeast China (Fig. 1, right). A total of 13,201 samples were collected during the period 2014–2017.

B) Snow survey courses (*Dataset 2*): A field campaign supported by the Chinese snow survey (CSS) project was conducted from December 2017 to March 2018 (Wang et al., 2018). During the field experiment period, a large number of snow pits were measured every 10 to 20 km. These measurements include snow depth, density, air temperature, and the stratigraphy of the snowpack. Fig. 1 shows the four snow survey routes in northern Xinjiang and Northeast China. Table 1 shows the details of the snow course data, including longitude, latitude, air temperature, snow depth, snow density and snow class. Snow course 1 was located in northern Xinjiang, around the Junggar Basin, which is dominated by grassland and bare ground. Snow course 2 was located around the Tian Shan Mountains and the Yili Valley, where the mean elevation exceeds 2000 m (Fig. 1). Following the definition by Sturm et al. (1995), snow cover in Xinjiang belongs to the prairie snow class, with the exception of the Altai Mountains (taiga and tundra) (Table 1). Snow course 3 was in eastern Inner Mongolia, from Xilingol (grassland) to the Great Khingan (forest). The major climatological snow classes are prairie, taiga and tundra (Table 1). There were two loop routes in dense forested areas for snow course 4, around the Changbai mountainous and lesser Khingan mountainous areas. The snow classes are mainly taiga and alpine (Table 1).

C) Field sampling work (*Dataset 3*): A field campaign from January to March 2018 supported by the CSS project was organized to densely measure snowpack parameters (snow depth and snow density) in fixed area grids (25 × 25 km^2) that could be used as standard sites to validate remotely sensed SWE products. However, these initially designed sampling grids were not exactly matched with the satellite pixels (e.g., Equal-Area Scalable Earth Grid (25 km × 25 km), hereafter, EASE-Grid) due to some inaccessible areas. Thus, dense measurements in a sampling grid could cover several spaceborne pixels. Fig. 2 shows the corresponding satellite pixels in northern Xinjiang and Northeast China. All samples are distributed in nonforested areas. The lack of forest cover makes the site an ideal study area for snow product validation. There were 4 ~ 25 measurements per pixel, including snow depth and snow density. Snow depth transect measurements were performed on January 21 and 23, February 1 and March 9, 2018. For field sampling, measurements within each grid cell were averaged to represent the ground truth SWE. All the true ground SWE data span from 4.6 mm to 66.7 mm. GlobSnow-2 product was generated using the Special Sensor Microwave Imager Sounder (SSMIS) brightness temperature data in EASE-Grid (25 km × 25 km) projection from 2010 to present (see Section 2.2). The standard AMSR2 SWE product was downloaded from JAXA's website (http://gcom-w1.jaxa.jp), and its pixel size is 0.25°×0.25°, different from GlobSnow-2's (Fig. 2). The standard FY-3D SWE product has been provided by CMA (http://data.cma.cn/en) since 2019. Thus, in this study, we utilized AMSR2 brightness temperature data (0.25° × 0.25°) but with FY-3D algorithms to retrieve SWE estimates during the period 2014–2018. Fig. 2 shows two kinds of satellite pixels (SSMIS: 25 km × 25 km; AMSR2: 0.25° × 0.25°). We collected 14 and 32 samples corresponding to the SSMIS (for GlobSnow-2) and AMSR2 pixels, respectively. Because of mountain masking and missing data, available samples for the GlobSnow-2 product are small compared to those of other products.

2.2. Various SWE algorithms

The GlobSnow-2 SWE historical dataset from 1979 to present is freely available (www.globsnow.info). The GlobSnow methodology was thoroughly presented by Pulliainen (2006) and Takala et al. (2011) (see Table 2). This product uses daily brightness temperatures (at 19 and 37 GHz in vertical polarization) from different satellite sensors: the Scanning Multichannel Microwave Radiometer (SMMR) from 1979 to 1987, the Special Sensor Microwave/Imager (SSM/I) from 1987 to 2009, and the SSMIS from 2010 to present.

The snow depth retrieval algorithm originally proposed by Chang et al. (1987) was designed for SMMR sensor. It is based on a linear regression between snow depth and the brightness temperatures gradient at ~ 19 and ~ 37 GHz (Table 2). In this study, we used SSMIS brightness temperature data available from the National Snow and Ice Center (NSIC, https://daacdata.apps.nsidc.org/pub/DATASETS) to retrieve snow depth estimates during the period 2014–2018.

The AMSR2 SWE product (L3) was downloaded from JAXA's Globe Portal System (http://gcom-w1.jaxa.jp). The current AMSR2 snow depth algorithm is an evolution of the original AMSR-E SWE algorithm and takes advantage of the expanded range of channels, such as 10.65, 18.7 and 36.5 GHz (Table 2). This algorithm retrieves the SWE from moderate snow accumulations using the 36.5 GHz channel and from deep snow using the 18.7 and 10.65 GHz channels.

China's FY-3D satellite was launched on 15 November 2017 with the goal of observing global atmospheric and geophysical features (http://satellite.nsmc.org.cn/portalsite/default.aspx?currentculture = en-US). The current FY-3D snow depth algorithm is an advancement from the original FY-3B mixed-pixel method. Due to different snow cover characteristics and land cover types in China's stable snow cover areas, regional algorithms were developed in Northeast China, Xinjiang, and other areas, respectively (Table 2). Due to no available standard FY-3D SWE product in CMA until 2019, in this study, the AMSR2 brightness temperature data (http://gcom-w1.jaxa.jp) were used to produce the FY-3D SWE product during the period 2014–2018.

2.3. Variable snow density

Snow density defines the relationship between snow depth and SWE. Density also largely determines the permittivity of dry snow and thus also affects the extinction rate of microwaves (Mätzler, 1987). For the GlobSnow-2 product, snow density is treated with a constant value of 240 kg/m^3, which is considered a reasonable 'global' value (Takala et al., 2011). For Chang's algorithm, the relationship between snow

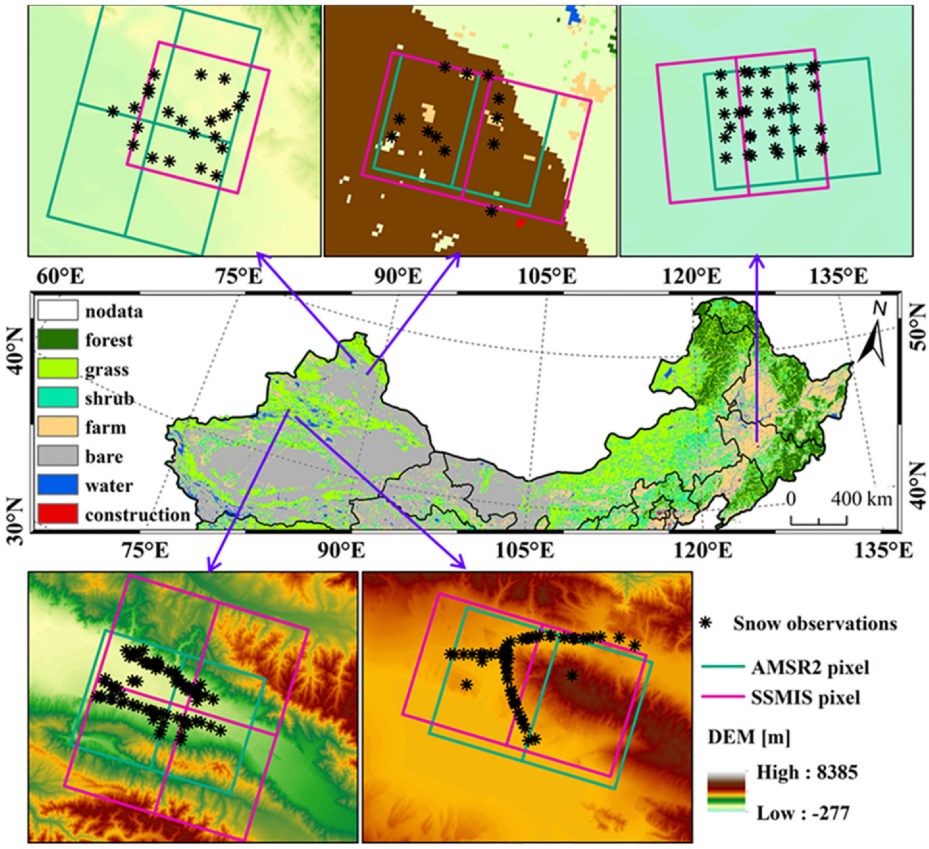

Fig. 2. The spatial distribution of field sampling measurements (black points) and satellite pixels in Xinjiang and Northeast China. The green and magenta lines represent AMSR2 and SSMIS pixels, respectively.

depth and brightness temperature gradient was fitted based on snow emission modeling (assuming snow density 300 kg/m^3). However, our previous study has demonstrated that Chang's algorithm presents serious overestimation in China (Yang et al., 2019). Thus, a constant snow density (240 kg/m^3) was used to convert snow depth to SWE for Chang SWE product in this study. According to the in situ data, the snow density is generally approximately 180 kg/m^3 in China, which is adopted in the FY-3D SWE product (Yang et al., 2019). The AMSR2 retrieval scheme utilizes the reference snow density of Sturm's climatological snow classes to yield SWE. However, snow bulk density is known to increase with time and depth as the weight of the overlying snow compacts the underlying layers (Kojima, 1966). Thus, regardless of snow depth, location, or time of year, these assumptions are not realistic, which could result in SWE estimation bias (Sturm and Wagner, 2010). To solve these problems, a statistical model based on a Bayesian analysis was presented by Sturm and Wagner in 2010. The bulk density is a function of snow depth, day of year (DOY), and snow climate class:

$$\rho_{h_i,DOY_i} = (\rho_{\max} - \rho_0)[1 - \exp(-k_1 \times h_1 - k_2 \times DOY_i)] + \rho_0 \quad (1)$$

where ρ_{max}, ρ_0, k_1, and k_2 are model parameters (DOY); these values vary with snow climate class; and i indicates the ith observation. Given that a snow season generally spans two calendar years, thus DOY ranges from −92 (1 October) to +181 (30 June, next year), with no 0 value.

2.4. Land cover fraction

The 1-km land use/land cover (LULC) data derived from the 30-m Thematic Mapper (TM) imagery classification was downloaded from the Data Center for Resources and Environmental Sciences, Chinese Academy of Sciences (http://www.resdc.cn/). The land cover types include grassland, cropland, forest, barren, water and construction (Fig. 2). The fraction was recalculated as the areal percentages of each

Table 2
Various snow depth retrieval algorithms used in this study.

Algorithm	Methodology	Basic format	Reference
GlobSnow-2	assimilation	$\min_{d_0}\{[Tb_{19V,HUT} - Tb_{37V,HUT}] - [Tb_{19V,satellite} - TB_{37V,satellite}]\}^2$ $\min_{D_t}\left(\frac{\{[Tb_{19V,HUT} - Tb_{37V,HUT}] - [Tb_{19V,satellite} - TB_{37V,satellite}]\}^2}{\sigma^2} + \left\{\frac{D_t - \hat{D_{ref,t}}}{\lambda D,\ ref,t}\right\}^2\right)$	Pulliainen, 2006; Takala et al., 2011
Chang	regression	$SD = 1.59 \times (Tb_{19H} - TB_{37H})$	Chang et al., 1987
AMSR2	regression	$SD = ff_{open} \times SD_{open} + ff_{forest} \times SD_{forest}$ $SD_{forest} = 1/log10(pol37) \times (Tb_{19V} - TB_{37V})/(1 - 0.6 \times fd)$ $SD_{open} = [1/log10(pol37) \times (Tb_{19V} - TB_{37V}) \times] + [1/log10(pol19) \times (Tb_{10V} - TB_{19V})]$	Kelly et al., 2003Kelly, 2009
FY-3D	regression	northeast China: $SD = 0.38 \times (Tb_{19H} - TB_{37H})/(1 - 0.7 \times ff)$ Xinjiang: $SD = 0.48 \times (Tb_{19V} - TB_{37H})$ Other regions: $SD = ff_{grass} \times SD_{grass} + ff_{forest} \times SD_{forest} + ff_{barren} \times SD_{barren} + ff_{farmland} \times SD_{farmland}$	Jiang et al., 2014; Yang et al., 2019

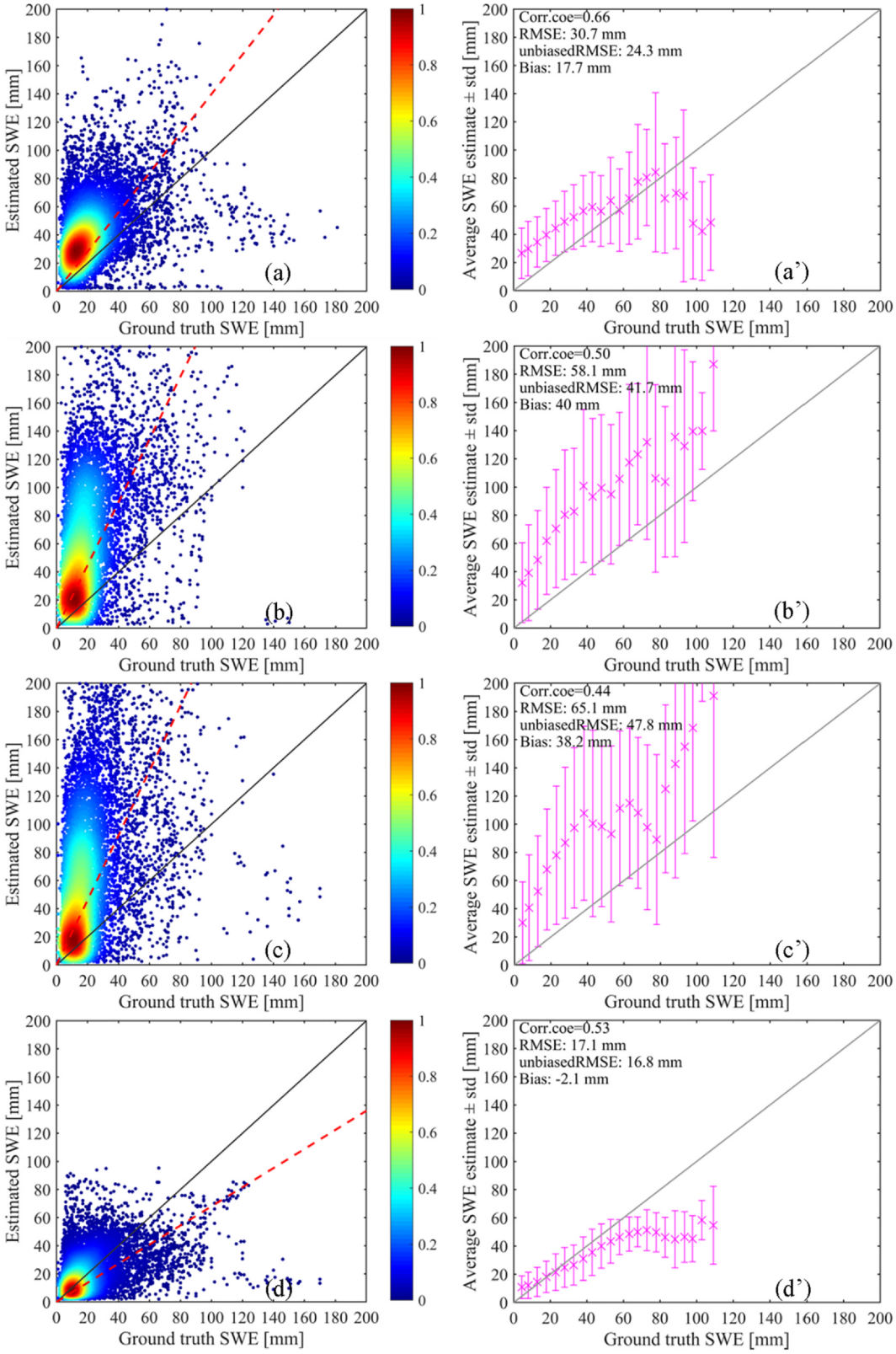

Fig. 3. Color-density scatterplots of estimated and measured SWE: (a) (a') GlobSnow-2; (b) (b') AMSR2; (c) (c') Chang; and (d) (d') FY-3D. The color scale represents the data density of scattered points, which range from 0 to 1. The red dotted line represents the linear fitting relationship.

land cover type in the corresponding satellite pixels. The pixels where the fraction of water bodies and construction is larger than 40% were filtered out.

3. Results

3.1. Product assessment

The GlobSnow-2 SWE estimates were evaluated using *datasets 1–3*. Meanwhile, to demonstrate the performance of the GlobSnow-2 estimates, it was compared with three other operational satellite SWE products.

3.1.1. Weather station observations (Dataset 1)

Fig. 3 shows scatter diagrams of estimated vs. measured values for all investigated SWE products. The accuracies of the AMSR2 and Chang SWE products are lower than those of the other products, with unbiased RMSEs of 41.7 mm and 48.7 mm, respectively (Fig. 3b and 3c). The retrievals of these products tend to be overestimated in terms of biases by approximately 40 mm, which is consistent with the results from Yang et al. (2015) and Gu et al. (2018) over China. For the Chang SWE product, the main reason for the overestimation is that the assumption regarding snow grain size (0.30 mm) fails in China (Li et al., 2014; Che et al., 2016). Although an empirical equation for the growth of snow grain size was included in the AMSR2 retrieval algorithm, it is found that there is only a slight improvement compared to the Chang algorithm, which is consistent with the previous studies (Kelly, 2009; Zhang et al., 2017; Yang et al., 2019). GlobSnow-2 SWE estimates outperform Chang and AMSR2 products (Fig. 3a). The unbiased RMSE and bias are equal to 24.3 mm and 17.7 mm, respectively, with the largest correlation coefficient (corr.coe) being 0.66. The GlobSnow-2 estimate is particularly underestimated when SWE exceeds the 80 mm threshold (Fig. 3a). However, for the SWE ranging from 0 to 50 mm, there is a slight overestimation (Fig. 3a). The FY-3D SWE retrieval scheme is designed for China, showing an unbiased RMSE of 16.8 mm (Fig. 3d). Although the mean bias is −2.1 mm, the FY-3D algorithm tends to

Table 3
The statistical results for SWE products with reference *dataset 2*. SC is the abbreviation of snow course. RPE represents the relative percentage error, which is calculated as RPE = abs(bias*100/SWE_{ground}).

Dataset	GlobSnow-2				
	corr.coe	RMSE (mm)	unRMSE (mm)	bias (mm)	RPE (%)
SC-1	0.39	19.0	14.7	12.2	55.9
SC-2	−0.14	23.6	23.8	3.8	13.1
SC-3	0.51	16.4	16.4	−1.8	6.5
SC-4	0.52	23.3	22.0	8.5	28.7
Total	0.36	19.8	19.3	4.8	17.7
	AMSR2				
SC-1	0.11	39.5	35.3	18.4	79.2
SC-2	0.30	40.8	37.2	17.7	44.1
SC-3	0.48	54.9	31.2	45.3	161.4
SC-4	0.54	45.1	27.1	36.2	122.8
Total	0.35	47.5	34.6	32.7	109.3
	Chang				
SC-1	0.31	64.1	40.8	49.9	220.4
SC-2	0.30	75.0	46.4	59.4	156.9
SC-3	0.57	96.1	45.4	84.3	307.3
SC-4	0.17	62.6	40.0	48.5	156.6
Total	0.38	79.3	46.4	64.4	221.8
	FY-3D				
SC-1	0.31	17.3	16.6	5.6	24.9
SC-2	0.28	22.1	20.6	−8.4	22.3
SC-3	0.67	22.4	18.3	13.0	47.5
SC-4	0.37	17.3	16.9	4.7	15.1
Total	0.42	20.3	19.4	5.7	19.8

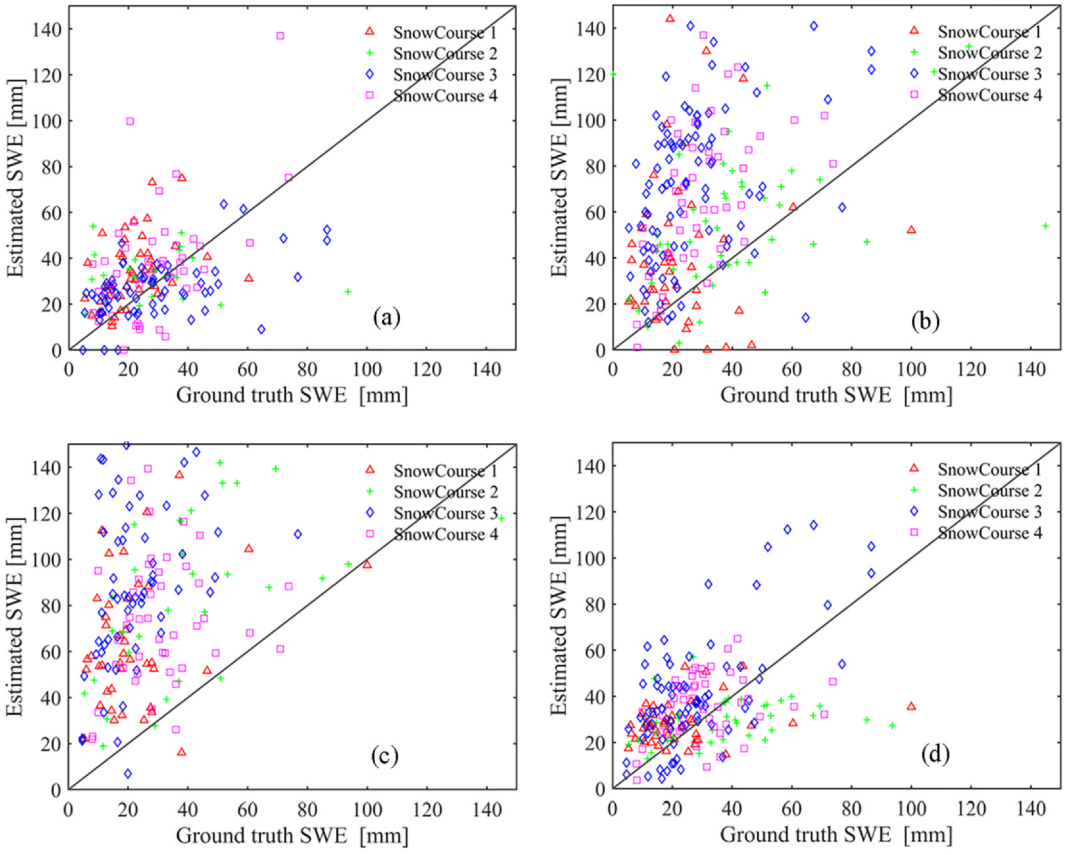

Fig. 4. Scatter diagrams of estimated vs. true SWE (a) GlobSnow-2; (b) AMSR2; (c) Chang; and (d) FY-3D.

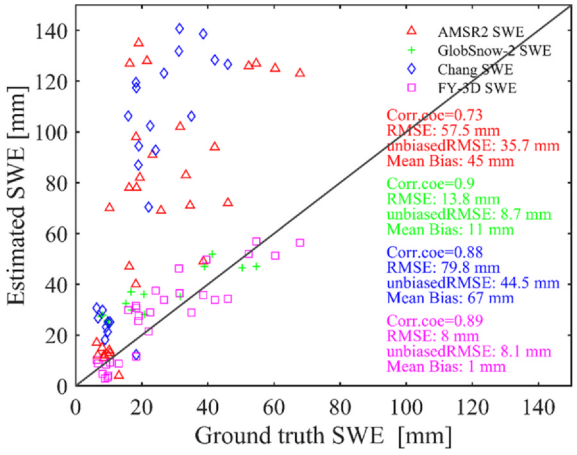

Fig. 5. SWE product performance over China versus densely sampled field measurements.

underestimate SWE for values exceeding 50 mm (Fig. 3d).

3.1.2. Field snow course survey (Dataset 2)

Fig. 4 shows the validation results of four satellite SWE products against snow course observations, with statistics given in Table 3. AMSR2 and Chang SWE values are overestimated, with mean biases of 32.7 mm and 64.4 mm, respectively. The relative percentage errors (RPE) in Table 3 are as high as 109.3% and 221.8%, respectively. The GlobSnow-2 SWE estimates show the best performance among these four products (Table 3). The overall unbiased RMSE and bias are 19.3 mm and 4.8 mm, respectively.

Snow course 1 was located in areas of shallow snow cover, where the mean snow depth was 13.2 cm (Fig. 1, Table 1). For this course, GlobSnow-2 SWE shows an overestimation with a bias of 12.2 mm (RPE: 55.9%), while the FY-3D product performs relatively well, with a bias of 5.6 mm and RPE of 24.9% (Table 3).

Snow course 2 was located around the Tian Shan Mountains and Yili Valley (Fig. 1). The GlobSnow-2 bias and RPE are 3.8 mm and 13.1%, respectively, which are lower than the FY-3D estimates (−8.4 mm and 22.3%, respectively). However, the correlation coefficient for GlobSnow-2 is −0.14. Fig. 3a also shows that snow course 2 (green plus sign) has poor SWE variability.

The performance of GlobSnow-2 in snow course 3 is best among the four snow survey routes, with an RPE of 6.5%. The FY-3D product shows an overestimation with a bias of up to 13 mm and an RPE of 50% (Table 3). The RPEs for GlobSnow-2 and FY-3D in snow course 4 are 28.7% and 15.1%, respectively.

3.1.3. Field sampling (Dataset 3)

Field sampling work was conducted in open areas where the forest cover fraction was close to zero. We assume here that the average of sampling measurements in one SWE product grid cell represents the true SWE. Fig. 5 shows that GlobSnow-2 and FY-3D SWE estimates are superior to the other two products, with unbiased RMSEs of 8.7 mm and 8.1 mm, respectively. GlobSnow-2 has a larger bias (11 mm) than FY-3D (1 mm). Fig. 3 also demonstrates that FY-3D SWE outperforms the others considering the relatively shallow snow cover (< 50 mm). Notably, the SSMIS pixels are not fully spatially matched with AMSR2 grids, possibly affecting the results (Fig. 2).

3.2. Effects of land cover, elevation, and snow class on GlobSnow-2

Fig. 6 shows the analysis of GlobSnow-2 SWE compared with *dataset 1*. Fig. 6a illustrates that the monthly unbiased RMSE and bias are minimized for the months of November and December due to the shallow and fresh snow cover. The unbiased RMSE (~38 mm) in March is the largest in the snow season, which is related to deep and wet snow conditions at the end of the snow season.

Retrieval sensitivity to land cover types (barren, grassland, farmland and forest) is shown in Fig. 6b. Any pixel where the land cover fraction is greater than 85% is viewed as a pure land cover type (Jiang et al., 2014). The most serious SWE overestimation occurs in forested areas (bias of up to 23.6 mm), showing that the effects of dense forest canopy on the microwave signal have significant impacts on this product. However, the highest SWE uncertainties occur for grassland, with an unbiased RMSE of 27.8 mm. The ground truth mean SWE in grassland is highest, whereas the estimated maximum mean SWE occurs in forest (Fig. 6b). Thus, forest correction is still one of the main challenges in SWE estimations over forested areas.

For the GlobSnow-2 product, grid cells with a high variation in elevation were masked out because of known a priori poor algorithm performance in complex terrain (Takala et al., 2011). To investigate the potential impact of topography, the bias and unbiased RMSE according to station elevation (in m) are shown in Fig. 7. As the elevation increases, the unbiased RMSE has very weak variability, showing that the uncertainties caused by the elevation are low. However, there is a significant upward trend in the bias with increasing elevation, except for the areas where the elevation ranges from 1000 m to 2000 m. As

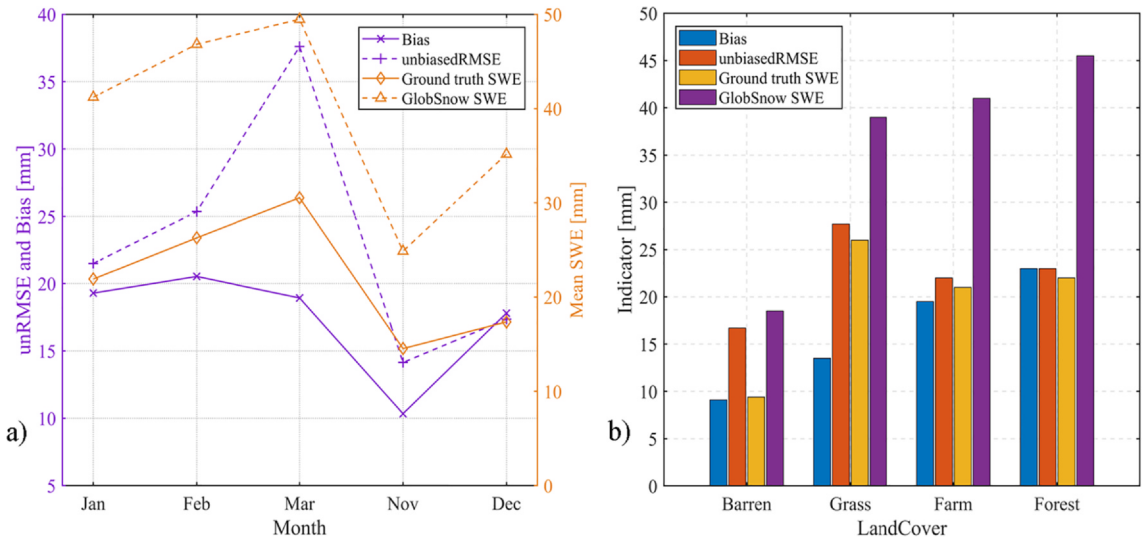

Fig. 6. The performance of the GlobSnow-2 SWE product according to the (a) monthly statistics and (b) land cover types.

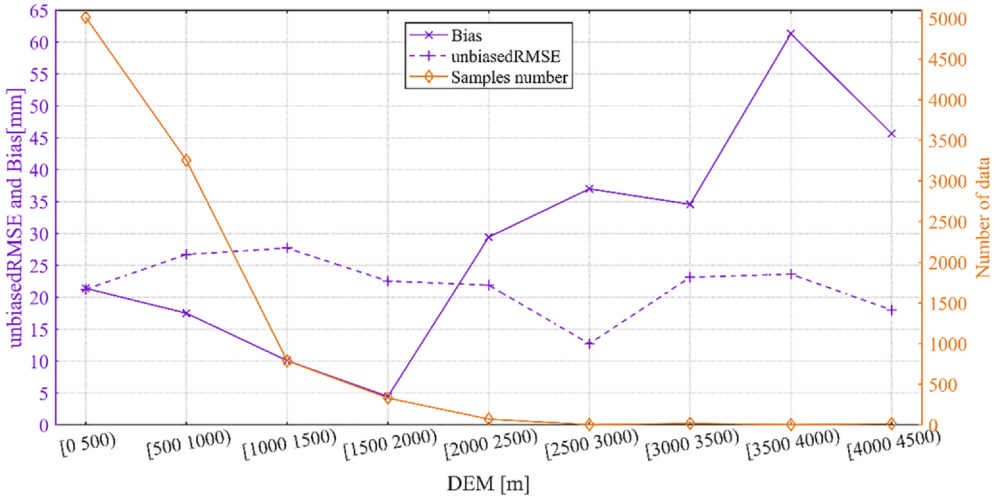

Fig. 7. The performance of the GlobSnow-2 SWE product as a function of the various elevations.

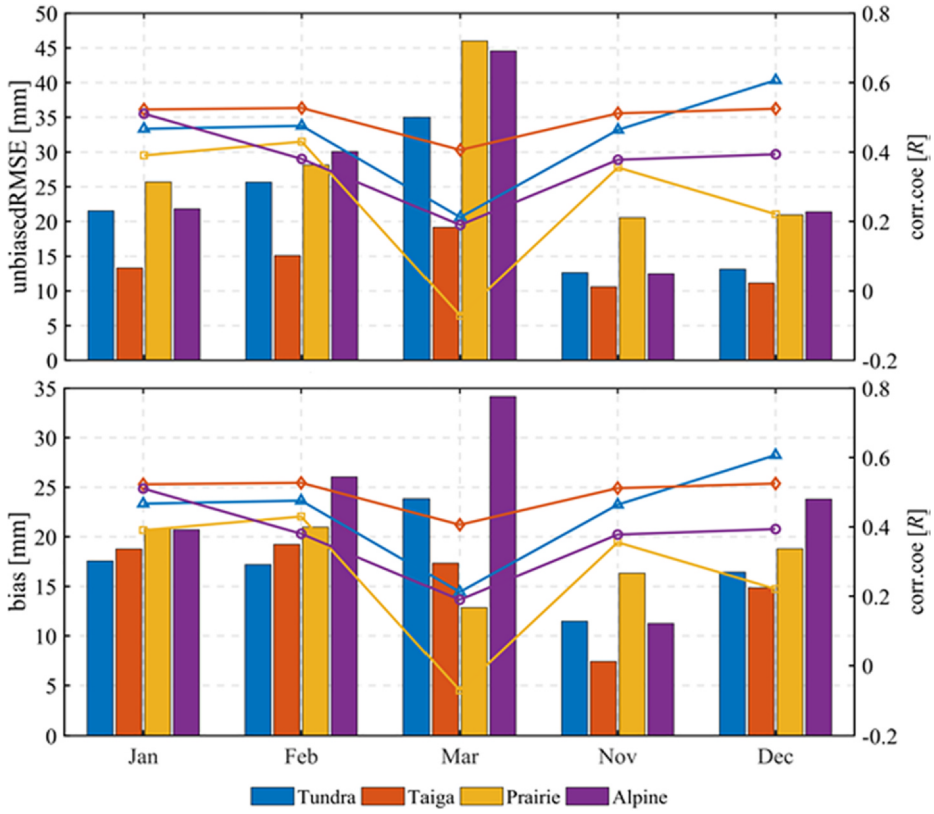

Fig. 8. Monthly SWE unbiased RMSE (top) and bias (bottom) variations in four snow classes. The corresponding lines represent the time series of the correlation coefficient.

Table 4
Overall statistical performances for each snow category.

Snow Class	Tundra	Taiga	Prairie	Alpine
corr.coe	0.45	0.50	0.27	0.37
bias (mm)	17.3	15.5	18.0	23.2
unRMSE (mm)	21.6	13.9	28.3	26.1

Table 5
Summary of overall performances for the GlobSnow-2 SWE product.

Index	Dataset 1 (station)	Dataset 2 (snow course)	Dataset 3 (field sampling)	Total
corr.coe	0.66	0.36	0.90	0.64
bias (mm)	17.70	4.80	11.00	11.17
RMSE (mm)	30.70	19.80	13.80	21.43
unRMSE (mm)	24.30	19.30	8.70	17.43
ERP (%)	62.32	17.70	44.40	41.47

shown in Fig. 1, the stations (green and yellow points) are mostly located in shallow snow cover areas, which explains why the bias in 1000–2000 m elevation range is small.

Fig. 8 displays the monthly mean unbiased RMSE, bias and

Table 6
Comparison of assessment results based on different research. Black bold numbers denote the accuracy compared with the snow course data; black bold italic numbers are for field sampling data; green bold numbers denote the validation in forested areas by Che et al. (2016).

Regions	Northern Xinjiang				Northeast China				China		
References	Dai et al., 2012	Zhang et al., 2017	Yang et al., 2019	This study	Che et al. 2016	Gu et al.2018	Yang et al., 2019	This study	Yang et al., 2019	This study
Chang SWE product										
RMSE (mm)	\	\	44.3	57.5 **(43.6)**	\	\	47.8	45.8 **(42.7)**	45.6	47.8 **(46.4)** ***(44.5)***
Bias (mm)	\	\	29.8	63.2 **(54.7)**	\	\	40.1	55.6 **(66.4)**	33.6	38.2 **(64.4)** ***(67.0)***
AMSR2 SWE product										
RMSE (mm)	41.3	34.3	37.6	44.4 **(36.3)**	23.7 **(41.2)**	59.7	40.8	39.1 **(29.2)**	38.4	41.7 **(34.6)** ***(35.7)***
Bias (mm)	26.6	12.0	10.8	12.2 **(18.1)**	13.2 **(30.1)**	57.6	23.8	21.7 **(40.8)**	20.9	40.0 **(32.7)** ***(45.1)***
FY-3D SWE product										
RMSE (mm)	\	\	\	20.8 **(18.6)**	\	\	\	15.1 **(17.6)**	15.8	16.8 **(19.4)** ***(8.1)***
Bias (mm)	\	\	\	1.4 **(−1.4)**	\	\	\	2.0 **(8.8)**	0.5	−2.1 **(5.7)** ***(1.1)***
GlobSnow-2 SWE product										
RMSE (mm)	26.8	\	\	33.1 **(19.3)**	8.8 **(10.6)**	\	\	19.5 **(19.2)**	\	24.3 **(19.3)** ***(8.7)***
Bias (mm)	17.0	\	\	3.2 **(8.1)**	3.9 **(−2.0)**	\	\	10.1 **(5.2)**	\	17.7 **(4.8)** ***(11.0)***

correlation coefficient of GlobSnow-2 SWE estimates compared with station observations (*dataset 1*) during the snowy winter seasons in the 2014–2017 period. The correlation is minimized for each snow category for the month of March, which is strongly related to snow humidity and snow metamorphism in the late snow season (Brun, 1989; Ebner et al., 2016; Kontu and Pulliainen, 2010). Generally, the GlobSnow-2 SWE product has a better performance for tundra and taiga snow classes than that in prairie and alpine snow cover (Table 4). There are high levels of uncertainties (unbiased RMSE, 28.3 mm) for prairie snow and serious overestimations (bias, 23.2 mm) for alpine snow (Table 4). It should be noted that the global Sturm's classification method may exhibit some uncertainty in China, possibly affecting the results.

4. Discussion

The overall unbiased RMSE and bias of the GlobSnow-2 product in China are 17.43 mm and 11.17 mm, respectively (Table 5). This accuracy level can meet most user requirements for SWE, such as water resource management (40 mm), climate analysis (30 mm), seasonal forecasting (30 mm) and climate model evaluation (30 mm) according to the ESA SnowConcepts study in 2017. However, we must note that snow cover is usually shallow over China, with a mean SWE of approximately 30 mm. The overall RPE for GlobSnow-2 is 41.7%, which by far exceeds the accuracy threshold (15%) of hydrological applications (Rott et al., 2010; Larue et al., 2017). Thus, overestimation is a key factor that affects the accuracy of GlobSnow-2 estimates in China.

The assessment results from different literatures are described in Table 6. The results show that the overall trends are consistent among these works in the literature. The global SWE products (AMSR2, Chang and GlobSnow-2) tend to overestimate SWE in China. For AMSR2 SWE product, it performs better in northern Xinjiang than in Northeast China, which is consistent with previous studies (Table 6). The validation results based on the station measurements, snow course data and field sampling observations (Section 2.1) also consistently present that the AMSR2 product typically overestimates SWE, with biases ranging from 32.7 to 45.1 mm. For the GlobSnow-2 product, there are notable differences when it is validated using different reference dataset, e.g., with the RMSEs of 24.3, 19.3 and 8.7 mm corresponding to the station, snow course and field sampling measurements, respectively. The comparison of performances in forested and open areas was conducted by Che et al. (2016) in Northeast China according to the in situ measurements observed by several stations. The RMSE in forested areas is larger than that in open areas, which is qualitatively consistent with the results in Fig. 6b. Snow course 3 and 4 are located in Northeast China, and dominated by forest (Figs. 1 and 2). The RMSE is 19.2 mm, larger than 10.6 mm in Che et al. (2016). The bias in our study is 5.2 mm, namely, slight overestimation, whereas it is opposite of the Che et al. (2016) result, with a bias of −2.0 mm. Please note that the study areas in the previous literature are not completely spatially matched with the regions defined in this paper. Moreover, the data amount and time range are not consistent each other, possibly effecting the result comparison.

Each snow class was defined by an ensemble of snow stratigraphic characteristics, including snow density, grain size, and morphologic crystals, which influence the snowpack microwave signature. Fig. 8 displays the good performance of GlobSnow-2 for both the tundra and taiga snow classes. Fig. 4 also indicates that GlobSnow-2 SWE estimates outperform the FY-3D product in terms of snow course 3. There are two major snow classes (taiga and tundra) along snow course 3 (Table. 1). Fig. 9 shows that the effective grain size optimized by the HUT model is larger in western Northeast China than in other areas. Moreover, the effective grain size presents an increasing trend from January to March 2018. The GlobSnow-2 assimilation model accounts for snow stratigraphy by the optimized effective snow grain size (Takala et al., 2011). The FY-3D retrieval method is a static semiempirical algorithm that is easily influenced by snow metamorphism and is not suitable for all

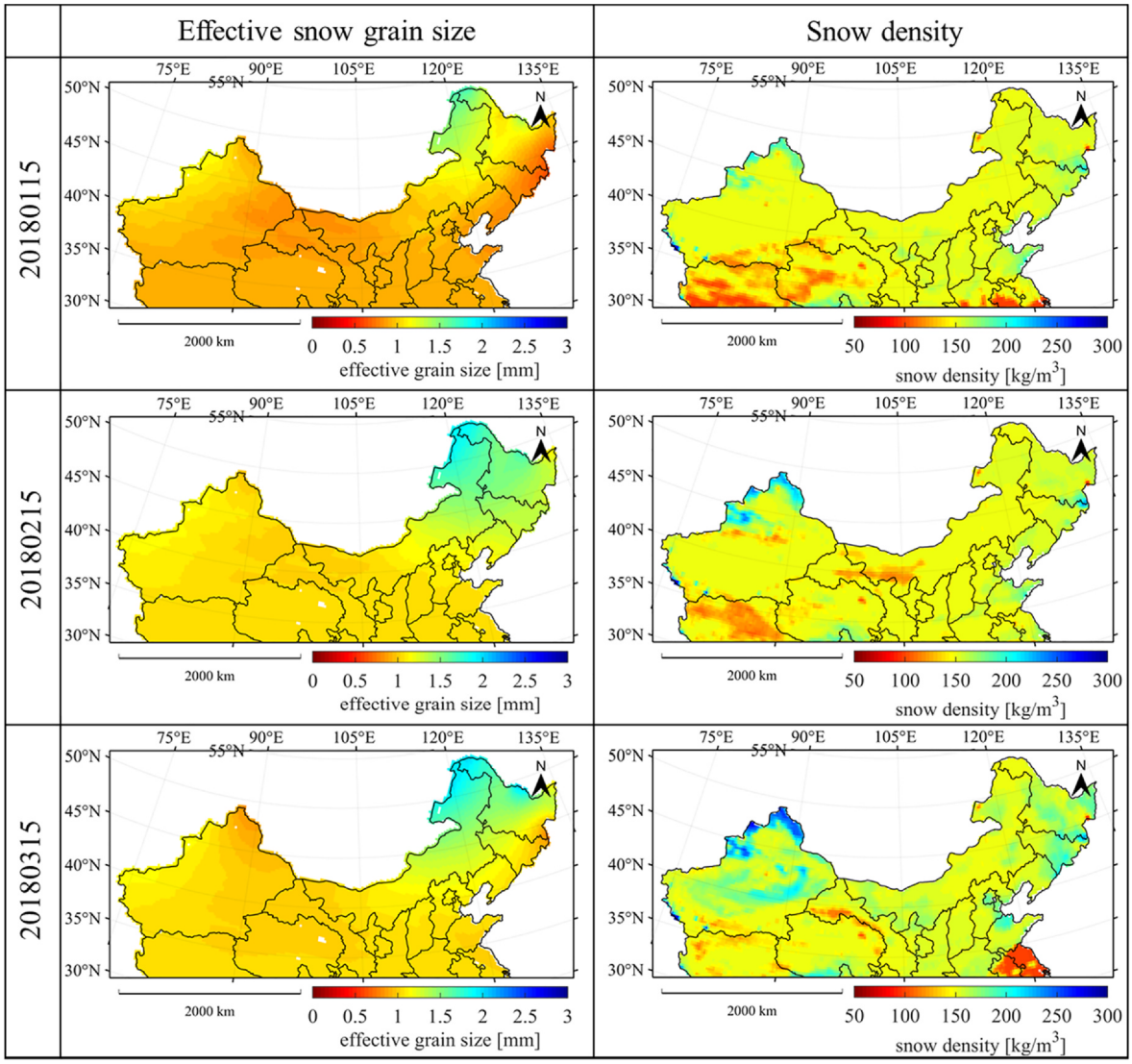

Fig. 9. Spatiotemporal patterns of effective snow grain size optimized by fitting the modeled brightness temperature into satellite observations and daily mean snow density from ERA5-land data (https://cds.climate.copernicus.eu/).

snow classes. The good performance of GlobSnow-2 and FY-3D in snow course 4, is partially attributable to the stable snowpack parameters (Fig. 4, Table 1). Fig. 9 also shows that the snow density in eastern Northeast China had no notable change during the January-March 2018 period.

Fig. 8 and Table 4 present a comparison of the performance for each snow class and indicate that the correlation coefficient for prairie snow is the lowest among the four major snow classes. One reason is that the temperature difference between day and night may increase the speed of metamorphism processes (Sturm and Wagner, 2010; Ebner et al., 2016). Another is that the presence of liquid water late in the spring, when snow is melting, typically results in higher absorption and poor penetration depth. Thus, GlobSnow-2 SWE estimates present the highest SWE uncertainties in March, with an unbiased RMSE of 45.7 mm for the prairie class. Fig. 6b also shows that the unbiased RMSE is 28 mm for grassland, which mainly covers prairie snow. Meanwhile, the GlobSnow-2 product overestimates SWE, particularly for alpine snow, with the highest bias of 34.2 mm in March (Fig. 8). Alpine snow cover is mostly distributed in eastern Northeast China, where there is dense forest and complex mountain topography (Changbai Mountains and lesser Khingan Mountains). As shown in Fig. 6b, the overestimation is as high as 23 mm in forested areas due to snow-vegetation interactions and vegetation contributions (emissions and transmissions). A previous study demonstrated that there is a significant upward trend in the unbiased RMSE according to the forest percentage in a satellite grid (25 km × 25 km), described as a simple quadratic function (Larue et al., 2017). For GlobSnow-2 product, the original equation by Kruopis et al. (1999) was applied to retrieve forest transmissivity. Moreover, a constant stem volume of 80 m^3/ha was applied because that there were no reliable global stem volume datasets at the time. The latest released GlobSnow-3 product adopted a revised algorithm proposed by Cohen et al. (2015) to simulate microwave attenuation in forest canopies. However, the transmissivity reaches saturation when the stem volume is larger than 100 m^3/ha (Cohen et al., 2015). Thus, it is difficult to achieve the desired correction effect with the revised algorithm in densely forested northeast China. Although previous studies have shown that the relationship between transmissivity and stem volume could be modeled as an exponential function (Langlois et al., 2011; Roy et al., 2014), this relationship is not clear because the transmissivity is not only related to the stem volume but also to the canopy closure, tree species, tree skin temperature and microwave frequency (Li et al., 2019).

Fig. 7 displays a significant upward trend in the bias with increasing elevation. Snow depth estimation in mountains (high altitude areas)

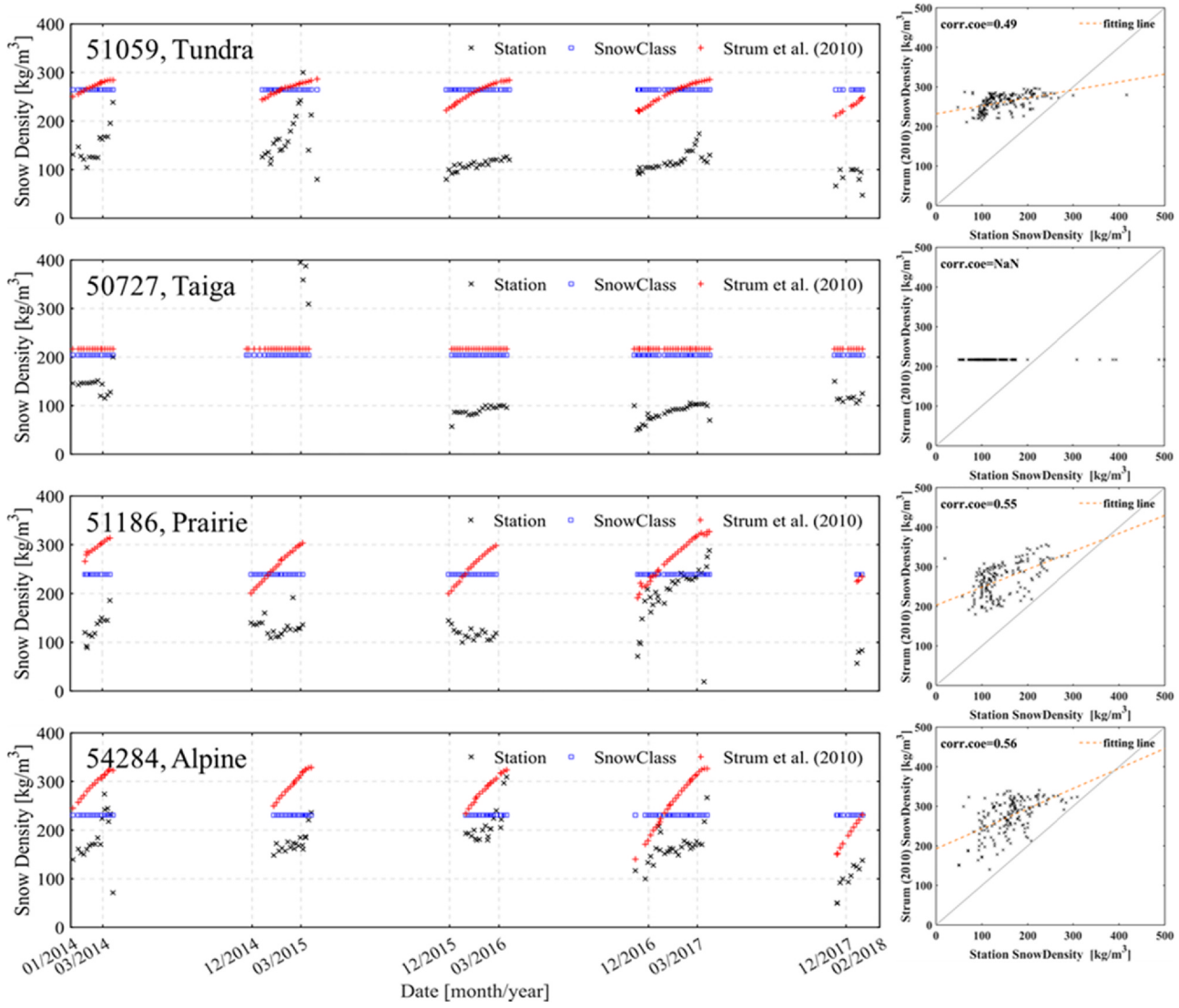

Fig. 10. Snow density daily time series from 2014 to 2017 for different snow classes. The right scatterplots represent the fitting relationship between the station measurement and estimated snow density with Sturm and Wagner (2010) for corresponding seasonal snow classification.

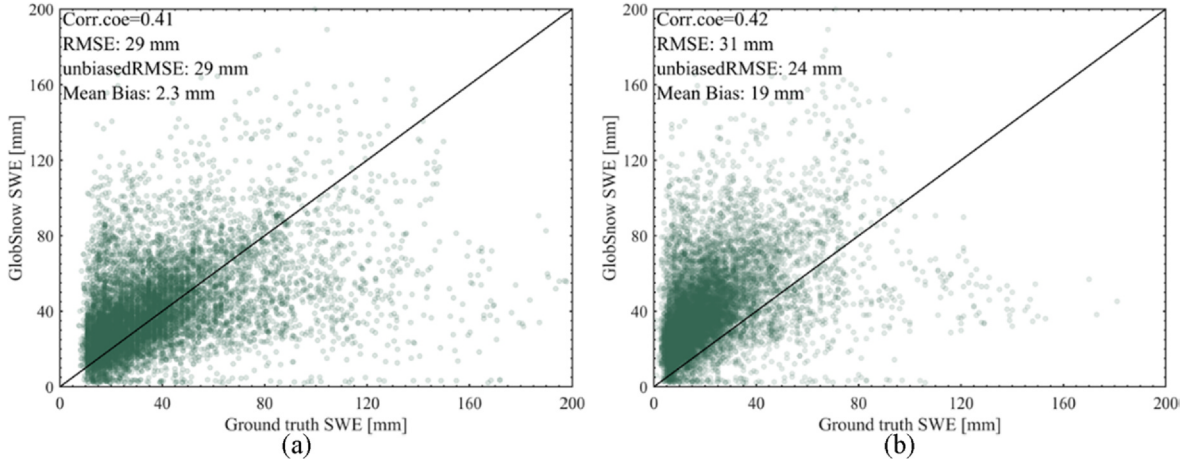

Fig. 11. Scatterplots between the GlobSnow-2 estimate and ground truth SWE calculated with (a) a fixed value of 240 kg/m^3 and (b) station-measured snow density.

remains a challenge because of the absence of ground truth data, poor representativeness of station observations, varied snow properties dramatically and high uncertainties in modeling (Lettenmaier et al., 2015; Dozier et al., 2016). Most of remotely sensed SWE products were generated using EASE-Grid data (25 km × 25 km), rather than raw PMW observations. In fact, the raw observation is finer than the resampled EASE-Grid data, although the satellite footprint is nominally elliptical. For instance, the AMSR-E's footprint size at 36.5 GHz is 8 km × 14 km, with an area of approximately 88 km^2 (Kelly, 2009). Some studies utilized AMSR-E Level 2A (L2A) brightness temperature product to characterize snow in mountainous areas, and results display that the L2A data are much more sensitive to ground-based SWE than the EASE-Grid data (Li et al., 2012; Santi et al., 2014).

Most SWE retrieval schemes are based on snow depth information because this variable can be directly measured at weather station. The GlobSnow-2 SWE retrieval scheme utilized a fixed density of 240 kg/m^3. Based on ground truth data, the average snow densities in Xinjiang and Northeast China are 190 kg/m^3 and 170 kg/m^3, respectively (Yang et al., 2019). Fig. 10 displays the time series of daily snow density, including station measurements, mean values for each snow class (Sturm et al., 1995), and modeling with a dynamic algorithm described in subsection 2.3. There are large differences among the three snow densities from the station, snow class and modeling. For the taiga snow class, the station snow density has almost no variation with the seasonal evolution. Taiga snow cover is distributed in northern Northeast China, with low air temperature and vapor pressure in the snow winter season (Ji et al., 2017). The temperature gradient between the snow and the atmosphere is small (Colbeck, 1982; Ebner et al., 2016). Moreover, snow cover is relatively shallow, and the metamorphism caused by compaction is nonsignificant. Thus, the snow density increases slowly with seasonal evolution. However, for the alpine snow class, the seasonal evolution of snow density is obvious. One reason is that these regions of alpine snow cover contain relatively high water vapor in the high latitudes in China (Shi et al., 2017; Ji et al., 2017). Another reason is that the temperature cycling between day and night may increase the speed of the processes (Ebner et al., 2016).

There is no doubt that using a fixed snow density or dynamic values from the model to convert snow depth to SWE will result in overestimation in China (Figs. 3, 4, 5). Fig. 11 compares the validation results using two different reference snow densities from station snow pressure observation and a fixed value (240 kg/m^3). Fig. 11a shows that the bias is only 2.3 mm when the ground truth SWE is a product of snow depth and fixed snow density, 240 kg/m^3. This is because the GlobSnow-2 retrieval algorithm treats snow density as a constant parameter. In the latest released GlobSnow-3 product, the snow density was still assumed to be 240 kg/m^3 (Pulliainen et al., 2020). However, a more objective bias in Fig. 11b is as high as 19 mm, showing a notable SWE overestimation in China. Thus, snow density is a key parameter that affects the accuracy level of the GlobSnow-2 SWE product.

5. Summary and conclusion

In this study, the GlobSnow-2 SWE product is evaluated using three reference validation datasets north of 35°N in China. The results show that GlobSnow-2 SWE estimates, which assimilate ground-based observations of snow depth and satellite observations, outperform the stand-alone satellite products, reducing the overall bias from 39.3 mm (57.5 mm) to 11.2 mm and unbiased RMSE from 37.3 mm (46.2 mm) to 17.4 mm compared with AMSR2 SWE (Chang SWE). The FY-3D SWE product, which was developed specifically for China, performs better than GlobSnow-2 for shallow snow conditions (< 50 mm), whereas an SWE exceeding 80 mm is typically underestimated. The retrieval sensitivity of GlobSnow-2 to land cover types has been studied in detail: the highest uncertainties are observed for grassland areas that cover several snow classes (taiga, tundra, prairie and alpine), with an unbiased RMSE of 28 mm. However, the bias in forest areas is the largest (23 mm) and overestimation is the most prominent among the four land cover types, showing that the effects of dense forest on the microwave signal still limit the accuracy of this product. GlobSnow-2 retrieval performance over diverse snow classes was also evaluated; the results show that GlobSnow-2 SWE estimates in taiga snow are generally superior to others. The overall unbiased RMSE and bias are 15.5 mm and 13.9 mm, respectively, with a correlation coefficient of 0.50. Relatively high uncertainties (unbiased RMSE, 28.3 mm) were found for prairie snow, and notable overestimation (bias, 23.2 mm) was found for alpine snow. In addition, the performance of the GlobSnow-2 SWE product was studied as a function of various elevations. The bias presents a significant upward trend, ranging from 5 mm to 61 mm with increasing elevation. The GlobSnow-2 assimilation approach tends to overestimate SWE, with biases of 17.7 mm, 4.8 mm and 11 mm for *datasets 1*, *2* and *3*, respectively. One of the major reasons is that the GlobSnow-2 SWE retrieval scheme utilized a fixed density of 240 kg/m^3, whereas a reasonable value for China according to ground truth data would be 180 kg/m^3. The results of this study also demonstrate that the spatially and temporally dynamic snow density model by Sturm and Wagner (2010) tends to overestimate snow density in China. This study evaluates the performance of the GlobSnow-2 SWE product in China and determines the major factors that affect the accuracy level of the assimilation scheme; the results will serve as a reference for us to improve the GlobSnow-2 SWE product in the near future.

CRediT authorship contribution statement

J.W. Yang: Methodology, Formal analysis, Visualization. **L.M. Jiang:** Conceptualization, Funding acquisition. **J. Lemmetyinen:** Formal analysis, Validation. **K. Luojus:** Methodology, Supervision, Software. **M. Takala:** Methodology, Supervision, Software. **S.L. Wu:** Investigation, Supervision. **J.M. Pan:** Supervision.

Declaration of Competing Interest

The authors declare that they have no known competing financial interests or personal relationships that could have appeared to influence the work reported in this paper.

Acknowledgments

This work was jointly supported by the Second Tibetan Plateau Scientific Expedition and Research Program [2019QZKK0206], the Science and Technology Basic Resources Investigation Program of China [2017FY100502], and the National Natural Science Foundation of China [41671334]. The authors thank the National Meteorological Information Center (http://data.cma.cn/en), the Data Center for Resources and Environmental Sciences Chinese Academy of Sciences (http://www.resdc.cn/), National Snow and Ice Data Center (https://nsidc.org/), and JAXA's Globe Portal System (http://gcom-w1.jaxa.jp) for providing the meteorological station measurements, land cover product, digital elevation model (DEM) data, and satellite datasets. We also thank all of our colleagues from the field campaign who supported the CSS project by performing the in situ measurements.

References

Armstrong, R., Brodzik, M., 2002. Hemispheric-scale comparison and evaluation of passive-microwave snow algorithms. Ann. Glaciol. 34, 38–44.
Bair, E.H., Abreu Calfa, A., Rittger, K., Dozier, J., 2018. Using machine learning for real-time estimates of snow water equivalent in the watersheds of Afghanistan. The Cryosphere 12, 1579–1594.
Barnett, T.P., Adam, J.C., Lettenmaier, D.P., 2005. Potential impacts of a warming climate on water availability in snow-dominated regions. Nature 438 (7066), 303–309.
Bartelt, P., Lehning, M., 2002. A physical SNOWPACK model for the Swiss avalanche warning: Part I: numerical model. Cold Reg. Sci. Technol. 35, 123–145.
Bormann, K.J., Brown, R.D., Derksen, C., Painter, T.H., 2018. Estimating snow-cover trends from space. Nat. Clim. Chang. 8, 924–928.

Brown, R.D., Robinson, D.A., 2011. Northern Hemisphere spring snow cover variability and change over 1922–2010 including an assessment of uncertainty. The Cryosphere. 5, 219–229.
Brun, E., 1989. Investigation on wet-snow metamorphism in respect of liquid-water content. Ann. Glaciol. 13, 22–26.
Cai, S., Li, D., Durand, M., Margulis, S.A., 2017. Examination of the impacts of vegetation on the correlation between snow water equivalent and passive microwave brightness temperature. Remote Sens. Environ. 193, 244–256.
Chang, A.T.C., Foster, J.L., Hall, D.K., 1987. Nimbus-7 SMMR derived global snow cover parameters. Ann. Glaciol. 9, 39–44.
Che, T., Li, X., Jin, R., Armstrong, R., Zhang, T., 2008. Snow depth derived from passive microwave remote-sensing data in China. Ann. Glaciol. 49, 145–154.
Che, T., Dai, L., Zheng, X., Li, X., Zhao, K., 2016. Estimation of snow depth from passive microwave brightness temperature data in forest regions of northeast China. Remote Sens. Environ. 183, 334–349.
Cohen, J., Lemmetyinen, J., Pulliainen, J., Heinilä, K., Montomoli, F., Seppänen, J., Hallikainen, M.T., 2015. The effect of boreal forest canopy in satellite snow mapping-A multisensor analysis. IEEE Trans. Geosci. Remote Sens. 53 (12), 6593–6607.
Colbeck, S.C., 1982. An overview of seasonal snow metamorphism. Rev. Geophys. 20 (1), 45–61.
Dai, L., Che, T., Wang, J., Zhang, P., 2012. Snow depth and snow water equivalent estimation from AMSR-E data based on a priori snow characteristics in Xinjiang. China. Remote Sens. Environ. 127, 14–29.
Dai, L., Che, T., Ding, Y., Hao, X., 2017. Evaluation of snow cover and snow depth on the Qinghai-Tibetan Plateau derived from passive microwave remote sensing. Cryosphere. 11, 1933–1948.
Dai, L., Che, T., Xie, H., Wu, X., 2018. Estimation of Snow Depth over the Qinghai-Tibetan Plateau Based on AMSR-E and MODIS Data. Remote Sensing. 10, 1989.
Derksen, C., Toose, P., Rees, A., Wang, L., English, M., Walker, A., Sturm, M., 2010. Development of a tundra-specific snow water equivalent retrieval algorithm for satellite passive microwave data. Remote Sens. Environ. 114, 1699–1709.
Derksen, C., Walker, A., Goodison, B., 2005. Evaluation of passive microwave snow water equivalent retrievals across the boreal forest/tundra transition of western Canada. Remote Sens. Environ. 96, 315–327.
Derksen, C., Brown, R., 2012. Spring snow cover extent reductions in the 2008–2012 period exceeding climate model projections. Geophys. Res. Lett. 39, 1–6.
Dozier, J., Bair, E.H., Davis, R.E., 2016. Estimating the spatial distribution of snow water equivalent in the world's mountains. WIREs Water 3, 461–474.
Durand, M., Kim, E.J., Margulis, S.A., 2009. Radiance assimilation shows promise for snowpack characterization. Geophys. Res. Lett. 36, L02503.
Durand, M., Liu, D., 2012. The need for prior information in characterizing snow water equivalent from microwave brightness temperatures. Remote Sens. Environ. 126, 248–257.
Ebner, P.P., Schneebeli, M., Steinfeld, A., 2016. Metamorphism during temperature gradient with undersaturated advective airflow in a snow sample. The Cryosphere. 10 (2), 791–797.
Forman, B.A., Reichle, R.H., 2015. Using a support vector machine and a land surface model to estimate large-scale passive microwave brightness temperatures over snow covered land in North America. IEEE J. Sel. Top. Appl. Earth Obs. Remote Sens. 8, 4431–4441.
Foster, J.L., Chang, A.T.C., Hall, D.K., 1997. Comparison of snow mass estimates from a prototype passive microwave snow algorithm, a revised algorithm and a snow depth climatology. Remote Sens. Environ. 62, 132–142.
Foster, J.L., Hall, D.K., Eylander, J.B., Riggs, G.A., Nghiem, S.V., Tedesco, M., Kim, E., Montesano, P.M., Kelly, R., Casey, K.A., Choudhury, B., 2011. A blended global snow producy using visible, passive microwave and scatterometer satellite data. Int. J. Remote Sens. 32, 1371–1395.
Foster, J.L., Sun, C., Walker, J.P., Kelly, R., et al., 2005. Quantifying the Uncertainty in Passive Microwave Snow Water Equivalent Observations. Remote Sens. Environ. 94 (2), 187–203.
Gelfan, A., Pomeroy, J., Kuchment, L., 2004. Modeling forest cover influences on snow accumulation, sublimation, and melt. J. Hydrometeorol. 5 (5), 785–803.
Gu, L., Ren, R., Li, X., 2016. Snow Depth Retrieval Based on a Multifrequency Dual-Polarized Passive Microwave Unmixing Method From Mixed Forest Observations. IEEE Trans. Geosci. Remote Sens. 54, 7279–7291.
Gu, L., Ren, R., Li, X., Zhao, K., 2018. Snow Depth Retrieval Based on a Multifrequency Passive Microwave Unmixing Method for Saline-Alkaline Land in the Western Jilin Province of China. IEEE J. Sel. Top. Appl. Earth Obs. Remote Sens. 11, 1–13.
Hallikainen, M.T., Ulaby, F.T., van Deventer, T.E., 1987. Extinction behavior of dry snow in the 18- to 90-GHz range. IEEE Trans. Geosci. Remote Sens. GRS. 25 (6), 737–745.
Hancock, S., Baxter, R., Evans, J., Huntley, B., 2013. Evaluating global snow water equivalent products for testing land surface models. Remote Sens. Environ. 128, 107–117.
Huang, X., Deng, J., Ma, X., Wang, Y., Feng, Q., Hao, X., Liang, T., 2016. Spatiotemporal dynamics of snow cover based on multisource remote sensing data in China. The Cryosphere. 10, 2453–2463.
Huang, X., Liu, C., Wang, Y., Feng, Q., Liang, T., 2019. Snow cover variations across China from 1952–2012. The Cryosphere Discuss. https://doi.org/10.5194/tc-2019-152.
Hansen, J., Nazarenko, L., 2004. Soot climate forcing via snow and ice albedos. Proc. Natl Acad. Sci. USA 101, 423–428.
Jeong, D., Sushama, L., Khaliq, M., 2017. Attribution of spring snow water equivalent (SWE) changes over the northern hemisphere to anthropogenic effects. Clim. Dyn. 48, 3645–3658.
Ji, D., Shi, J., Xiong, C., Wang, T., Zhang, Y., 2017. A total precipitable water retrieval method over land using the combination of passive microwave and optical remote sensing. Remote Sens. Environ. 191, 313–327.
L. Jiang J. Shi S. Tjuatja J. Dozier K. Chen L. Zhang A parameterized multiple-scattering model for microwave emission from dry snow Remote Sensing of Environment. 111 2007 357 366.
Jiang, L., Shi, J., Tjuatja, S., Chen, K., Zhang, L., Du, J., 2011. Estimation of Snow Water Equivalence Using the Polarimetric Scanning Radiometer from the Cold Land Processes Experiments (CLPX03). IEEE Geosci. Remote Sens. Lett. 8, 359–363.
Jiang, L., Wang, P., Zhang, L., Yang, H., Yang, J., 2014. Improvement of snow depth retrieval for FY3B-MWRI in China. Sci. China Earth Sci. 44, 531–547.
Kelly, R., Chang, A., Leung, T., Foster, L., 2003. A prototype AMSR-E global snow area and snow depth algorithm. IEEE Trans. Geosci. Remote Sens. 41, 230–242.
Kelly, R., 2009. The AMSR-E Snow Depth Algorithm: Description and Initial Results. Journal of The Remote Sensing Society of Japan. 29, 307–317.
Kim, R.S., Durand, M., Li, D., Baldo, E., Margulis, S.A., Dumont, M., Morin, S., 2019. Estimating alpine snow depth by combining multifrequency passive radiance observations with ensemble snowpack modeling. Remote Sens. Environ. 226, 1–15.
Densification of seasonal snow cover. Physics of Snow and Ice Vol. 1, 929–951.
Kontu, A., Pulliainen, J., 2010. Simulation of spaceborne microwave radiometer measurements of snow cover using in situ data and brightness temperature modeling. IEEE Trans. Geosci. Remote Sens. 48 (3), 1031–1044.
Kontu, A., Lemmetyinen, J., Vehviläinen, J., Leppänen, L., Pulliainen, J., 2017. Coupling SNOWPACK modeled grain size parameters with the HUT snow emission model. Remote Sens. Environ. 194, 33–47.
Kruopis, N., Praks, J., Arslan, A., Alasalmi, H., Koskinen, J., Hallikainen, M., 1999. Passive microwave measurements of snow-covered forests in EMAC'95. IEEE Trans. Geosci. Remote Sens. 37, 2699–2705.
Kwon, Y., Yang, Z.L., Hoar, T.J., Toure, A.M., 2017. Improving the Radiance Assimilation Performance in Estimating Snow Water Storage across Snow and Land-Cover Types in North America. J. Hydrometeor. 18, 651–668.
S. Kumar C. Peters-Lidard K. Arsenault A. Getirana D. Mocko Quantifying the Added Value of Snow Cover Area Observations in Passive Microwave Snow Depth Data Assimilation Journal of Hydrometeorology 16 4 2015 150428132421008.
Larue, F., Royer, A., DeSève, D., Langlois, A., Roy, A., Brucker, L., 2017. Validation of GlobSnow-2 snow water equivalent over Eastern Canada. Remote Sens. Environ. 194, 264–277.
Larue, F., Royer, A., De Sève, D., Roy, A., Picard, G., Vionnet, V., Cosme, E., 2018. Simulation and assimilation of passive microwave data using a snowpack model coupled to a well-calibrated radiative transfer model over North-Eastern Canada. Water Resour. Res. 54 (2), 1–26.
Langlois, A., Royer, A., Dupont, F., Roy, A., Goita, K., Picard, G., 2011. Improved corrections of forest effects on passive microwave satellite remote sensing of snow over boreal and subarctic regions. IEEE Trans. Geosci. Remote Sens. 49 (10), 3824–3837.
Langlois, A., Royer, A., Derksen, C., Montpetit, B., Dupont, F., Goïta, K., 2012. Coupling of the snow thermodynamic model SNOWPACK with the Microwave Emission Model for Layered Snowpacks (MEMLS) for subarctic and arctic Snow Water Equivalent retrievals. Water Resour. Res. 48, W12524.
Lemmetyinen, J., Derksen, C., Pulliainen, J., Strapp, W., Toose, P., Walker, A., 2009. A comparison of airborne microwave brightness temperatures and snowpack properties across the boreal forests of Finland and Western Canada. IEEE Trans. Geosci. Remote Sens. 47 (3), 965–978.
Lemmetyinen, J., Derksen, C., Toose, P., Proksch, M., Pulliainen, J., Kontu, A., Rautiainen, K., Seppänen, J., Hallikainen, M., 2015. Simulating seasonally and spatially varying snow cover brightness temperature using HUT snow emission model and retrieval of a microwave effective grain size. Remote Sens. Environ. 156, 71–95.
Lemmetyinen, J., Schwank, M., Rautiainen, K., Kontu, A., Parkkinen, T., Mätzler, C., Wiesmann, A., Wegmüller, U., Derksen, C., Toose, P., 2016. Snow density and ground permittivity retrieved from L-band radiometry: Application to experimental data. Remote Sens. Environ. 180, 377–391.
Lettenmaier, D., Alsdorf, D., Dozier, J., Huffman, G., Pan, M., Wood, E., 2015. Inroads of remote sensing into hydrologic science during the WRR era. Water Resour. Res. 51, 7309–7342.
Li, D., Durand, M., Margulis, S., 2012. Potential for hydrologic characterization of deep mountain snowpack via passive microwave remote sensing in the Kern River basin, Sierra Nevada, USA. Remote Sens. Environ. 125, 34–48.
Li, D., Durand, M., Margulis, S., 2017. Estimating snow water equivalent in a Sierra Nevada watershed via spaceborne radiance data assimilation. Water Resour. Res. 53, 647–741.
Li, W., Guo, W., Qiu, B., Xue, Y., Hsu, P.-C., Wei, J., 2018. Influence of Tibetan Plateau snow cover on East Asian atmospheric circulation at medium-range time scales. Nat. Commun. 9, 4243.
Li, Q., Kelly, R., Leppanen, L., Juho, V., Kontu, A., Lemmetyinen, J., Pulliainen, J., 2019. The Influence of Thermal Properties and Canopy-Intercepted Snow on Passive Microwave Transmissivity of a Scots Pine. IEEE Trans. Geosci. Remote Sens. 99, 1–10.
Li, X., Zhao, K., Wu, L., Zheng, X., 2014. Spatiotemporal analysis of snow depth inversion based on the FengYun-3B MicroWave Radiation Imager: a case study in Heilongjiang Province. China. Journal of Applied Remote Sensing. 8, 084692.
Magnusson, J., Winstral, A., Stordal, A.S., Essery, R., Jonas, T., 2017. Improving physically based snow simulations by assimilating snow depths using the particle filter. Water Resour. Res. 53 (2), 1125–1143.
Mätzler, C., 1987. Applications of the interaction of microwaves with the natural snow cover. Remote Sens. Rev. 2, 259–391.
Mätzler, C., 1994. Passive microwave signatures of landscapes in winter. Meteorog. Atmos. Phys. 54, 241–260.
Mudryk, L., Derksen, C., Kushner, P., Brown, R., 2015. Characterization of Northern Hemisphere Snow Water Equivalent Datasets, 1981–2010. J. Clim. 28, 8037–8051.
Mortimer, C., Mudryk, L., Derksen, C., Luojus, K., Brown, R., Kelly, R., Tedesco, M., 2020. Evaluation of long-term Northern Hemisphere snow water equivalent products. The

Cryosphere. 14, 1579–1594. https://doi.org/10.5194/tc-14-1579-2020.
Pan, J.M., Durand, M.T., Sandells, M., Lemmetyinen, J., Kim, E.J., Pulliainen, J., Kontu, A., Derksen, C., 2016. Differences between the HUT snow emission model and MEMLS and their effects on brightness temperature simulation. IEEE Trans. Geosci. Remote Sens. 54 (4), 2001–2019.
J.M. Pan M.T. Durand B.J. Vander Jagt D. Liu Application of a Markov Chain Monte Carlo algorithm for snow water equivalent retrieval from passive microwave measurements Remote Sensing of Environment. 192 2017 150 165.
Picard, G., Brucker, L., Roy, A., Dupont, F., Fily, M., Royer, A., Harlow, C., 2013. Simulation of the microwave emission of multi-layered snowpacks using the dense media radiative transfer theory: the DMRT-ML model. Geosci. Model Dev. 6 (4), 1061–1078.
Picard, G., Sandells, M., Löwe, H., 2018. SMRT: An active-passive microwave radiative transfer model for snow with multiple microstructure and scattering formulations (v1.0). Geosci. Model Dev. 11, 2763–2788.
Pulliainen, J., Kärnä, J.P., Hallikainen, M.T., 1993. Development of geophysical retrieval algorithms for the MIMR. IEEE Trans. Geosci. Remote Sensing. 31, 268–277.
Pulliainen, J., 2006. Mapping of snow water equivalent and snow depth in boreal and sub-arctic zones by assimilating space-borne microwave radiometer data and ground-based observations. Remote Sens. Environ. 101, 257–269.
Pulliainen, J., Aurela, M., Laurila, T., Aalto, T., Takala, M., Salminen, M., Kulmala, M., Barr, A., Heimann, M., Lindroth, A., 2017. Early snowmelt significantly enhances boreal springtime carbon uptake. Proc. Natl. Acad. Sci. USA 2017 (114), 11081–11086.
Pulliainen, J., Luojus, K., Derksen, C., et al., 2020. Patterns and trends of Northern Hemisphere snow mass from 1980 to 2018. Nature 581, 294–298. https://doi.org/10.1038/s41586-020-2258-0.
Qin, Y., Abatzoglou, J.T., Siebert, S., et al., 2020. Agricultural risks from changing snowmelt. Nat. Clim. Chang. 10, 459–465. https://doi.org/10.1038/s41558-020-0746-8.
Ran, Y., Li, X., Lu, L., Li, Z., 2012. Large-scale land cover mapping with the integration of multi-source information based on the Dempster-Shafer theory. International Journal of Geographical Information Science. 26, 169–191.
Rott, H., Yueh, S.H., Cline, D.W., Duguay, C., Essery, R., Haas, C., Hélière, F., Kern, M.G., Malnes, E., Nagler, T., Pulliainen, J., Rebhan, H., Thompson, A., 2010. Cold regions hydrology high-resolution observatory for Snow and Cold Land Processes. Proc. IEEE 98 (5), 752–765.
Roy, A., Goïta, K., Royer, A., Walker, A.E., Goodison, B.E., 2004. Snow water equivalent retrieval in a Canadian boreal environment from microwave measurements using the HUT snow emission model. IEEE Trans. Geosci. Remote Sens. 42 (9), 1850–1859.
Roy, A., Royer, A., Hall, R., 2014. Relationship Between Forest Microwave Transmissivity and Structural Parameters for the Canadian Boreal Forest. IEEE Geosci. Remote Sens. Lett. 11, 1802–1806.
Santi, E., Pettinato, S., Paloscia, S., Pampaloni, P., Macelloni, G., Brogioni, M., 2012. An algorithm for generating soil moisture and snow depth maps from microwave spaceborne radiometers. Hydrol. Earth Syst. Sci. 16, 3659–3676.
Santi, E., Pettinato, S., Paloscia, S., Pampaloni, P., Fontanelli, G., Crepaz, A., Valt, M., 2014. Monitoring. of Alpine snow using satellite radiometers and artificial neural networks. Remote Sens. Environ. 144, 179–186.
Shi, L.J., Qiu, Y.B., Shi, J.C., Lemmetyinen, J., Zhao, S.J., 2017. Estimation of Microwave Atmospheric Transmittance Over China. IEEE Geosci. Remote Sens. Lett. 99, 1–5.
Stigter, E.E., Wanders, N., Saloranta, T.M., Shea, J.M., Bierkens, M.F.P., Immerzeel, W.W., 2017. Assimilation of snow cover and snow depth into a snow model to estimate snow water equivalent and snowmelt runoff in a Himalayan catchment. The Cryosphere. 11, 1647–1664.
Sturm, M., Holmgren, J., Liston, G.E., 1995. A seasonal snow cover classification system for local to global applications. J. Clim. 8, 1261–1283.
Sturm, M., Wagner, A.M., 2010. Using repeated patterns in snow distribution modeling: An arctic example. Water Resour. Res. 46, 65–74.
Sun, C., Walker, J.P., Houser, P.R., 2004. A methodology for snow data assimilation in a land surface model. J. Geophys. Res. 109, D08108.
Tedesco, M., Kelly, R., Foster, J.L., Chang, A.T.C., 2004. AMSR-E/Aqua Daily L3 Global Snow Water Equivalent EASE-Grids. Version 2. NASA National Snow and Ice data center Distributed Active Archive Center, Boulder, Colorado USA. Doi: 10.5067/AMSR E/AE_DYSNO.002.
Tedesco, M., Kim, E.J., 2006. Intercomparison of electromagnetic models for passive microwave remote sensing of snow. IEEE Trans. Geosci. Remote Sens. 44 (10), 2654–2666.
Tedesco, M., Narvekar, P., 2010. Assessment of the NASA AMSR-E SWE product. IEEE J. Sel. Top. Appl. Earth Obs. Remote Sens. 3 (1), 141–159. https://doi.org/10.1109/JSTARS.2010.2040462.
Takala, M., Luojus, K., Pulliainen, J., Lemmetyinen, J., Juha-Petri, K., Koskinen, J., Bojkov, B., 2011. Estimating northern hemisphere snow water equivalent for climate research through assimilation of space-borne radiometer data and ground-based measurements. Remote Sens. Environ. 115, 3517–3529.
Vander Jagt, B., Durand, M., Margulis, S., Kim, E., Molotch, N., 2015. On the characterization of vegetation transmissivity using LAI for application in passive microwave remote sensing of snowpack. Remote Sens. Environ. 156, 310–321.
Vormoor, K., Lawrence, D., Heistermann, M., Bronstert, A., 2015. Climate change impacts on the seasonality and generation processes of floods – projections and uncertainties for catchments with mixed snowmelt/rainfall regimes. Hydrol. Earth Syst. Sci. 19, 913–931.
Wang, J., Che, T., Li, Z., Li, H., Hao, X., Zheng, Z., Xiao, P., Li, X., Huang, X., Zhong, X., Dai, L., Li, H., Ke, C., Li, L., 2018. Investigation on snow characteristics and their distribution in China. Advances in Earth Science. 33, 12–26.
Wang, Y., Huang, X., Wang, J., Zhou, M., Liang, T., 2019. AMSR2 snow depth downscaling algorithm based on a multifactor approach over the Tibetan Plateau. China. Remote Sensing of Environment. 231, 111268.
X. Xu J. Li B.A. Tolsonv Progress in integrating remote sensing data and hydrologic modeling 2014 Prog. Phys Geog 0309133314536583.
Xue, Y., Forman, B.A., 2017. Atmospheric and Forest Decoupling of Passive Microwave Brightness Temperature Observations Over Snow-Covered Terrain in North America. IEEE Journal of Selected Topics in Applied Earth Observations & Remote Sensing. 10, 3172–3189.
Xue, Y., Forman, B.A., Reichle, R.H., 2018. Estimating snow mass in North America through assimilation of Advanced Microwave Scanning Radiometer brightness temperature observations using the Catchment land surface model and support vector machines. Water Resour. Res. 54, 6488–6509.
Yang, J., Jiang, L., Ménard, C.B., 2015. Evaluation of snow products over the Tibetan Plateau. Hydrol. Process. 29, 3247–3260.
Yang, J., Jiang, L., Wu, S., Wang, G., Wang, J., Liu, X., 2019. Development of a Snow Depth Estimation Algorithm over China for the FY-3D/MWRI. Remote Sensing 11, 977.
Yang, J., Jiang, L., Luojus, K., Pan, J., Lemmetyinen, J., Takala, M., Wu, S., 2020. Snow depth estimation and historical data reconstruction over China based on a random forest machine learning approach. The Cryosphere. 14, 1763–1778.
Zhang, R.P., Liang, T.G., Feng, Q.S., Huang, X.D., Wang, W., Xie, H.J., Guo, J., 2017. Evaluation and Adjustment of the AMSR2 Snow Depth Algorithm for the Northern Xinjiang Region, China. IEEE J. Sel. Top. Appl. Earth Obs. Remote Sens. 10 (9), 3893–3903.
Zheng, X.M., Li, X.F., Jiang, T., Ding, Y.L., Wu, L.L., Zhang, S.Y., Zhao, K., 2016. Retrieving soil surface temperature under snowpack using special sensor microwave/imager brightness temperature in forested areas of Heilongjiang, China: an improved method. J. Appl. Remote Sens. 10 (2), 26016.
Zhong, X., Zhang, T., Kang, S., Wang, K., Zheng, L., Hu, Y., Wang, H., 2018. Spatiotemporal variability of snow depth across the Eurasian continent from 1966 to 2012. The Cryosphere. 12, 227–245.